ISSN 1392-1207. MECHANIKA. Vol. 32, No. 1, 2026: 68–79

# Simulation and Optimization for Hot Stamping Process of Rear Windshield Lower Crossbeam of Aluminum Alloy Automobiles

**Huijun ZHAO*, Jiarui XU*, Jianghua HUANG**, Yang XIAO*, Haibing FU***, Binghe JIANG****

*Hangzhou Dianzi University, No.1158, 2 Street, Baiyang Street, Qiantang District, Hangzhou 310018, Zhejiang Province, China, E-mails: zhaohuijun@hdu.edu.cn, 23010702@hdu.edu.cn, 21011427@hdu.edu.cn

**Zhejiang University of Science and Technology, No.318, Liuhe Road, Xihu District, Hangzhou 310023, Zhejiang Province, China, E-mails: huangjianghua@zust.edu.cn (Corresponding Author), hjh79303416@126.com

***Zhejiang Zhaofeng Mechanical and Electronical CO., LTD., No.6, Zhaofeng Road, Qiaonan Block, Xiaoshan District, Hangzhou 311232, Zhejiang Province, China, E-mail: fhb@hzfb.com

https://doi.org/10.5755/j02.mech.40111

## 1. Introduction

In recent years, the rapid progress of the automotive industry has led to increasingly conspicuous issues regarding resource scarcity and environmental pollution [1, 2]. According to statistics, if the vehicle weight is reduced by 10%, the fuel efficiency can rise by 6-8%, and the emissions can be diminished by 4% [3]. Given that new energy vehicles are not yet fully mature and conventional engine technology is becoming increasingly challenging to upgrade, automotive lightweighting undoubtedly constitutes the most efficacious measure for energy conservation and emission reduction. The weight of the vehicle body accounts for approximately 40% of the total vehicle weight, and the lightweighting of the vehicle body plays a crucial role in the lightweighting of the vehicle [4, 5]. Aluminum alloy is regarded as a material with significant potential for automotive lightweighting due to its advantages such as low density, high specific strength and stiffness, favorable impact resistance, strong corrosion resistance, and excellent recyclability [6, 7]. For instance, the Audi A8 adopted an all-aluminum body, which not only enhanced the torsional rigidity of the body by 60% but also reduced the weight of the car by 50% compared to the steel body of similar models [5]. Therefore, aluminum alloy body forming has become an effective measure of automotive lightweight, and has been widely used in the automotive manufacturing industry.

Aluminum alloy has poor room-temperature forming plasticity, limited deep drawing ability, significant part rebound, and difficult control of dimensional accuracy. With the increase in deformation temperature, the plasticity of aluminum alloy sheets improves significantly, and the forming capacity enhances significantly [8]. Currently, the hot forming process is commonly applied to the manufacturing of aluminum alloy components, especially for body parts with complex shapes and high dimensional accuracy, which are mostly formed through hot stamping [9]. Zhang et al. [10] conducted simulation analysis and experimental research on the hot stamping process of the A-pillar welded sheet of aluminum alloy and investigated the influence of process parameters on the formability of the parts. Wang et al. [11] studied the deformation characteristics of the AA6082 welded sheet with different thickness combinations during hot forming-quenching (HFQ). Harrion et al. [12] verified the feasibility of hot stamping the B-column outer plate of 7075 high-strength aluminum alloy through experimental research. Zhou et al. [13] analyzed the defects in the stamping forming of the anti-collision beams of aluminum alloy automotives. Jiang et al. [14] optimized and analyzed the process parameters of the hot stamping forming of the rear windshield lower crossbeam in 6016 aluminum alloy automobiles.

The hot stamping of aluminum alloy is a combination of hot forming and heat treatment. The forming process undergoes a dynamic temperature process, and the thermal deformation mechanism is relatively complex. For this reason, many researchers have conducted numerous theoretical modeling and experimental studies [15-17]. Fan et al. [18] investigated the forming mechanism of the 6A02 aluminum alloy sheet using a hot-forming die at the deformation temperature of 50-350°C, revealing the microstructure evolution and strengthening mechanism of the forming process. Wang et al. [19] studied the formability and failure mechanism of AA2024 aluminum alloy hot-forming at 350-493°C, and described the corresponding relationship between the formability of the aluminum alloy and temperature. Gu et al. [20] employed high-temperature tensile tests and Nakazima experiments to simulate the HFQ process to study the high-temperature rheological behavior and formability of 7075-T4 aluminum alloy. Jiang et al. [21] studied the quenching sensitivity of 7046A aluminum alloy through end-quenching tests and examined the mechanical properties and microstructure of the aged alloy. Jiang et al. [22] studied the influence of HFQ process conditions on the microstructure evolution and baking hardening effect of AA7075.

However, there are many factors affecting the hot stamping process of aluminum alloy; the forming process is complicated; and the experimental research is costly and the cycle is long. In recent years, finite element simulation technology has been widely employed in the research of the hot stamping process [23-27]. Xiao et al. [28] carried out experimental verification on the simulation of the deep drawing at high temperature and studied the effects of the forming temperature, stamping speed, blank holding force, and friction coefficient on the formability and mechanical properties of 7075 aluminum alloy. Ma et al. [29] studied the influence of the friction coefficient on the minimum thickness, thickness deviation, and failure mode of AA6111 aluminum alloy hot-stamping parts by combining finite element analysis and experimental verification. Ghiotti et al. [30] investigated the influence of process parameters such as the forming temperature and normal contact pressure on the friction

behavior during AA7075 hot stamping through finite element simulation. Li et al. [31] utilized numerical and experimental methods to study the effects of process parameters such as the forming temperature, blank holding force, die size, and local thickening of sheets on the residual stress distribution of hot stamping aluminum alloy parts. Additionally, with the development of computer technology, various advanced mathematical modeling methods are gradually applied to the optimization of process parameters [9, 32]. Jens et al. [33] used a variety of machine learning methods to model the deformation behavior of 7075 aluminum alloy, such as support vector machine, gradient lift, random forest, ridge regression, lasso regression, adaptive enhanced regression model, extreme gradient lift, multi-layer perceptrons, etc. It was found that the extreme gradient lifting model was the most advantageous in modeling the deformation behavior of aluminum alloy. Xie et al. [34] proposed an improved hybrid model based on the constrained Boltzmann machine and backpropagation neural network, established the mapping relationship between process parameters and forming quality, and used the multi-objective particle swarm optimization algorithm to perform multi-objective optimization of the hot stamping process parameters. Liu et al. [35] established a general IHTC model applicable to hot and warm stamping of aluminum alloys and integrated it with the CCP diagram to determine the key process parameters during hot/warm stamping of aluminum alloys. However, the forming performance of aluminum alloy parts is affected by multiple process parameters, including forming temperature, friction coefficient, stamping speed, blank holding force, die size, etc. Different forming processes and forming methods directly impact the forming quality of the parts. Therefore, the combination of finite element simulation and algorithm optimization is an effective measure to optimize the forming process and performance prediction of aluminum alloy auto body parts under complex process conditions.

Based on this, the rear windshield lower crossbeam of an aluminum alloy automobile was taken as the research object in this paper. The hot stamping process scheme of the part was optimized by finite element simulation. The modular hot stamping die that can realize different forming methods was designed and developed, and the simulation results were verified by the hot stamping experiment of the rear windshield lower crossbeam. The influence of process parameters such as deformation temperature, friction coefficient, stamping speed, and die clearance on part thinning under two forming methods was analyzed through simulation. The gradient boosting regression tree machine learning model and NSGA-II algorithm were used to optimize the hot stamping process parameters of the part. This research can provide a significant reference value for the selection and optimization of hot stamping process for aluminum alloy auto body parts.

## 2. Hot Stamping Finite Element Modeling

The dimensions of the rear windshield lower crossbeam of aluminum alloy automobiles are shown in Fig. 1, a, and the thickness of the sheet is 1.5 mm. Fig. 1, b shows the die surface diagram designed according to the geometry structure of the part. The finite element geometry model of the rear windshield lower crossbeam hot stamping is shown in Fig. 2.

6016 aluminum alloy was selected as the part material with a density of 2.7 kg/m³ and a Poisson's ratio of 0.3. The stress-strain curve at high temperatures was obtained through thermal physical simulation experiments overheating in the previous research, as shown in Fig. 3. The sheet mesh was generated using Belytschko-Tsay shell elements through automatic meshing, with maximum element sizes of 20 mm and minimum sizes of 5 mm, employing a fourth-order adaptive optimization coefficient. The die material used was H13 steel. Given the minimal mold deformation, it was treated as a rigid body in this model, with maximum element sizes of 5 mm and minimum sizes of 1 mm. The final meshing results include 529 sheet elements, 31,398 upper die elements, and 35,470 lower die elements. During the hot stamping of the rear windshield lower crossbeam, the sheet temperature can reach up to 550°C. The initial temperature of the die was only 10°C (The die adopted a water-cooled system). The temperature disparity between the mold and the sheet material fosters contact heat transfer between them. In order to ensure the accuracy of the finite element simulation, the heat transfer coefficient between the die and the sheet needs to be defined. The heat transfer coefficient at the interface contact between the die and the sheet can be effected by the interfacial pressure and distance. During hot stamping, the interaction forces and clearance between the sheet and die will vary with deformation. As the contact interface pressure increases and clearance decreases, the thermal conductivity coefficient rises, as shown in Table 1 [36, 37]. Based on this, a thermal contact model between the sheet and die was established. In the hot stamping simulation, the punch was constrained in the vertical direction until contacting the sheet metal, while other displacements were set to zero. The concave die remained stationary throughout the process, meaning it was subjected to a fully fixed constraint.

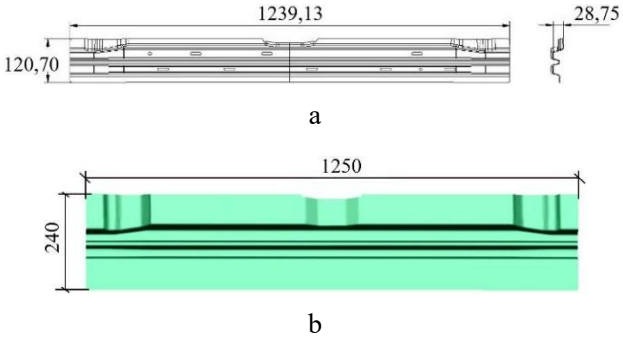


Fig. 1 Rear windshield lower crossbeam: a – dimensional diagram of part, b – die surface diagram

The one-step direct forming process was first tried, and the forming process parameters were set as follows: forming temperature 510°C, friction coefficient 0.15, stamping speed 50 mm/s, mold clearance 1.05t (t is the thickness of sheet metal). The thickness distribution and temperature distribution of the rear windshield lower crossbeam were obtained by simulation, as shown in Fig. 4. It can be seen from Fig. 4, a that the maximum thickness of the part reached 1.899 mm, with a maximum thickness increase rate of 26.6%. Meanwhile, the minimum thickness was measured at 0.904 mm, showcasing a maximum thinning rate of 39.7%, which meant that the part had cracked and failed. The obvious thinning areas were concentrated in the

middle of the cross section of the rear windshield lower crossbeam. This phenomenon was attributed to the non-uniform size distribution of the cross section, making the convex position in the middle of the cross section prone to cracking. Fig. 4, b demonstrated that upon completion of stamping, the lowest temperature of the part was approximately 344°C, and the highest temperature reached around

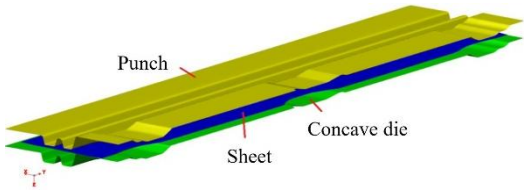


Fig. 2 Finite element geometry model of rear windshield lower crossbeam hot stamping

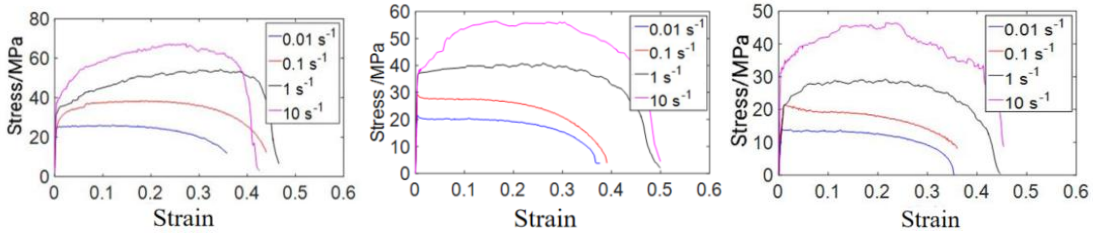


a b c

Fig. 3 True stress-strain curves of 6016 aluminum alloy at high temperature deformation: a – 450°C, b – 500°C, c – 550°C

Table 1

The relationship between coefficient of heat conduction, pressure and clearance of aluminum alloy sheet and die

| Pressure, MPa | Coefficient of heat conduction, W/m²·K | Clearance, mm | Coefficient of heat conduction, W/m²·K |
|---|---|---|---|
| 0 | 0 | 6 | 0 |
| 10 | 50 | 5 | 0.5 |
| 20 | 55 | 4 | 0.65 |
| 40 | 60 | 2 | 1 |
| 50 | 60 | 0 | 3 |


a

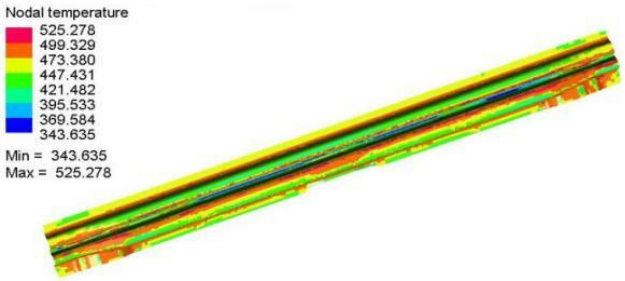


b

Fig. 4 Simulation results of rear windshield lower crossbeam using one-step forming: a – thickness distribution, b – temperature distribution

525°C. The temperature in most areas was maintained between 400°C and 500°C, indicating the part remained in a high temperature state even post-stamping.

## 3. Hot Stamping Process Optimization

### 3.1. Optimization simulation

To address the concerns regarding potential cracking or excessive thinning of the rear windshield lower crossbeam during one-step forming, a stepwise forming process plan was devised. This method was divided into two forming steps: initially preforming the middle section of the parts, followed by stamping the two sides of the parts. The finite element geometric model of two-step forming is shown in Fig. 5, a. The forming process is executed as follows: the concave die (inside) can be pushed out to the highest plane of the concave die (outside) about 50 mm. As the punch moved down, the middle convex position of the part was pre-formed, and then the concave die (inside) moved downward with the punch to complete the stamping on both sides of the part. The shape change of the sheet during the two-step forming process is illustrated in Fig. 5, b.

The forming process parameters were also set to forming temperature 510°C, friction coefficient 0.15, stamping speed 50 mm/s, mold clearance 1.05t. Using the two-step forming process, the thickness and temperature distributions were simulated, as shown in Fig. 6. It can be seen from Fig. 6, a that the maximum thickness of the two-step formed part was 1.807 mm and the maximum thickening rate was 20.5%, and the minimum thickness was 1.277 mm and the maximum thinning rate was 14.9%. The maximum thickening rate decreased by 6.1% and the maximum thinning rate decreased by 24.8% compared with the one-step forming. The thickness distribution of the part showed a good consistency, which effectively avoided the phenomenon that the middle convex position of the part was easy to crack. Fig. 6, b illustrates that after stamping, the temperature of most areas ranged between 300°C and 400°C, with the highest temperature recorded at approximately 417°C and the lowest at around 45°C, primarily concentrated in the

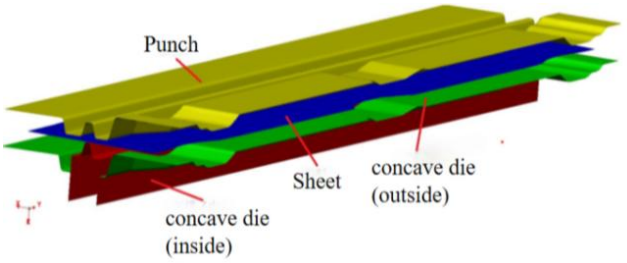


a


b

Fig. 5 The two-step forming process of rear windshield lower crossbeam: a – finite element geometric model, b – part shape change process


a


b

Fig. 6 Simulation results of rear windshield lower crossbeam using two-step forming: a – thickness distribution, b – temperature distribution

middle convex position. This phenomenon was due to the continued contact of the middle convex position with the die after forming, facilitating a quicker temperature drop. And because of the effect of heat conduction, the temperature of the two-step formed parts was significantly lower than that of the one-step formed parts, which can further improve the efficiency of quenching while using the die forming.

### 3.2. Experimental verification

The hot stamping die of the rear windshield lower crossbeam of aluminum alloy automobile is shown in Fig. 7. The upper and lower die cores used split assembly structure, which was conducive to the cooling pipe processing. In order to achieve a one-step forming and two-step forming at the same time, the middle part of the die was designed as a moving block. During the one-step forming, the bottom surface of the middle moving block was parallel to the plane of the fixed block of the lower die. During the two-step forming, the middle moving block of the lower die was pushed out by using the ejecting cylinder of the press. The ejection height can be adjusted up to 350 mm. The upper and lower dies were each equipped with two inlet and two outlet ports for cooling water, which was maintained at approximately 10°C.

The materials used in the experiment were 6016-T6 aluminum alloy sheets with a thickness of 1.5 mm produced by Southwest Aluminum (Group) Co., Ltd. The stamping speed was 50 mm/s, graphite lubricant was used on the sheet surface and the die surface (friction coefficient was close to 0.15), the holding time was 8 min, the transfer time and the pressure holding time were 10 s, and the forming temperature was 480°C, 510°C, 540°C and 570°C. As shown in Fig. 8, a, the qualified rear windshield lower crossbeam forming parts were finally obtained by two-step stamping. However, the convex position in the middle of the part would crack by the one-step stamping, as shown in Fig. 8, b.

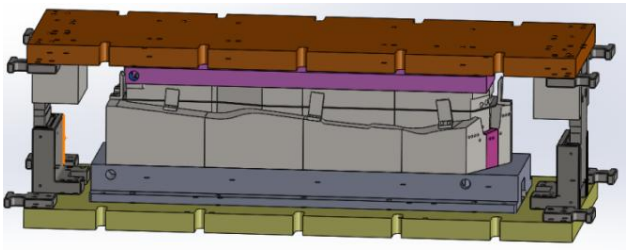

a

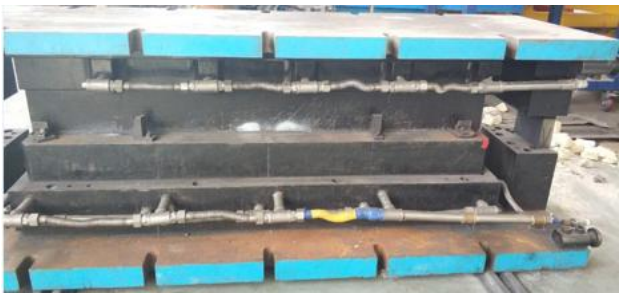

b

Fig. 7 Hot stamping die for the rear windshield lower crossbeam of automobiles: a – design drawing, b – physical view

To further validate the reliability of the finite element simulation results, the thickness size of the section position depicted in Fig. 9 was measured. The wire cutting machine was used to cut the cross-section 130 mm from the left end of the part, and the thickness of the cross-section position was measured by Vernier caliper. The average value of the data of each point was taken from three times of measurement, and the thickness of the cross-section was obtained in 29 points. The thickness of the section at the same position was extracted from the finite element simulation results. The comparison between the simulation results and experi-

mental results at a forming temperature of 510°C is illustrated in Fig. 10. The findings indicate that the simulation outcomes closely align with the experimental data, with some minor deviations observed at the transition corners of the section. These variations could be attributed to forming errors and measurement inaccuracies easily occurred in the position of transition corners. For the selected section, the minimum thickness of the part appeared at the position

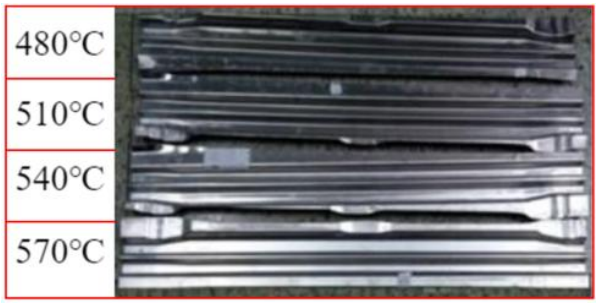


a

b

Fig. 8 Formed parts: a – two-step formed parts, b – the fracture location of the parts using one-step forming

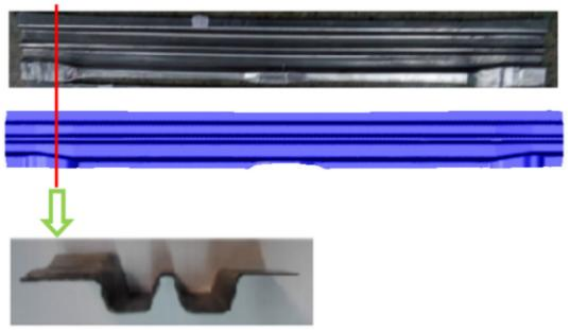

Fig. 9 Section position of rear windshield lower crossbeam

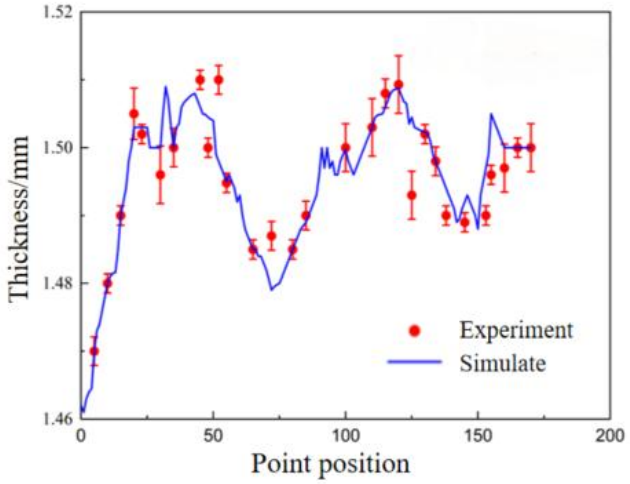


Fig. 10 Section thickness distribution of parts

where the leftmost end of the section is concave. Additionally, a noticeable thinning phenomenon was also observed at the bottom of the part section.

Comparing simulation predictions with experimental results under two forming methods revealed that both methods consistently predicted fracture occurrence in one-step formed parts, with fracture locations (at the central raised area) matching simulation predictions. The two-step forming method achieved qualified parts across different temperatures. As shown in Fig. 10, the formed part at 510°C exhibited a maximum cross-sectional thickness of 1.512 mm and a minimum of 1.469 mm, while the simulation model predicted a maximum thickness of 1.508 mm and a minimum of 1.461 mm, with an error margin within 1%. This demonstrates that the developed finite element simulation model for aluminum automotive rear windshield crossbeams can effectively predict part formability, providing guidance for process selection and optimization.

## 4. Influence of Process Parameters on Part Thickness

During the hot stamping of aluminum alloy, the process parameters such as deformation temperature, friction coefficient, stamping speed, and die clearance play significant roles in the forming quality of parts. In this study, the influence of the above process parameters on the minimum thickness of the part under single factor variables was studied by the finite element simulation, using the one-step stamping and the two-step stamping respectively. The specific process parameters are shown in Table 2.

Table 2

Hot stamping simulation process scheme

| No. | Forming temperature, °C | Friction coefficient | Stamping speed, mm/s | Die clearance, mm |
|---|---|---|---|---|
| 1 | 480/510/540/570 | 0.3 | 200 | 1.10t |
| 2 | 540 | 0.15/0.3/0.45/0.6 | 200 | 1.10t |
| 3 | 540 | 0.3 | 50/100/150/200 | 1.10t |
| 4 | 540 | 0.3 | 200 | 1.05t/1.10t/1.15t/1.20t |

The effects of process parameters on the minimum thickness of the rear windshield lower crossbeam of aluminum alloy using different forming processes are illustrated in Fig. 11. Under the same process conditions, the choice of forming method had a significant influence on the thickness of parts, and the minimum thickness of the two-step formed parts was greater than that of the one-step formed parts.

Fig. 11, a shows the curves of the minimum thickness of the rear windshield lower crossbeam of aluminum alloy automobile under different deformation temperatures. At the same deformation temperature, the minimum thickness of parts with the two-step forming was greater than that with one-step forming. This meant that the maximum thinning rate of parts with the two-step forming was lower than

that with one-step forming. Across the temperature range of 480-570°C, the maximum thinning rate of the parts remained around 15% using one-step forming, with only minor fluctuations. As a contrast, when the deformation temperature was lower than 540°C, the change value of the minimum thickness of the part was less than 0.01 mm, and the maximum thinning rate was not more than 9% using the two-step forming. But the maximum thinning rate of the two-step formed part increased to 12% at 570°C.

Fig. 11, b shows the variation curves of the minimum thickness of the rear windshield lower crossbeam of aluminum alloy automobiles with different friction coefficients. After the aluminum alloy sheet is heated, the surface viscosity increases, resulting in an increase in the friction coefficient between the sheet and the die. Under the same friction coefficient, the minimum thickness of the two-step formed parts was greater than that of the one-step formed parts. With the increase of friction coefficient, the minimum thickness decreased and the maximum thinning rate increased. Compared with the two-step forming, the friction coefficient had a significant effect on the thinning of the parts using the one-step forming. When the friction coefficient was 0.15, the maximum thinning rate of the parts under the two forming methods was about 9%, and the difference was not much. However, with the increase of friction coefficient, the curve of minimum thickness of the one-step formed part decreased sharply. When the friction coefficient was 0.6, the minimum thickness of the one-step formed part was 0.95 mm, and the maximum thinning rate reached 37%, while the maximum thinning rate of the two-step formed part was only 12%.

Fig. 11, c shows the change curves of the minimum thickness of the rear windshield lower crossbeam of aluminum alloy automobiles at different stamping speeds. At the same stamping speed, the minimum thickness of the two-step formed parts was greater than that of the one-step formed parts, that is, the maximum thinning rate of the two-step formed parts was lower than that of the one-step formed parts. Taking the stamping speed of 150 mm/s as an example, the maximum thinning rate of the part is 24% using one-step forming, and the maximum thinning rate of the part is 12% using two-step forming. With the increase of the stamping

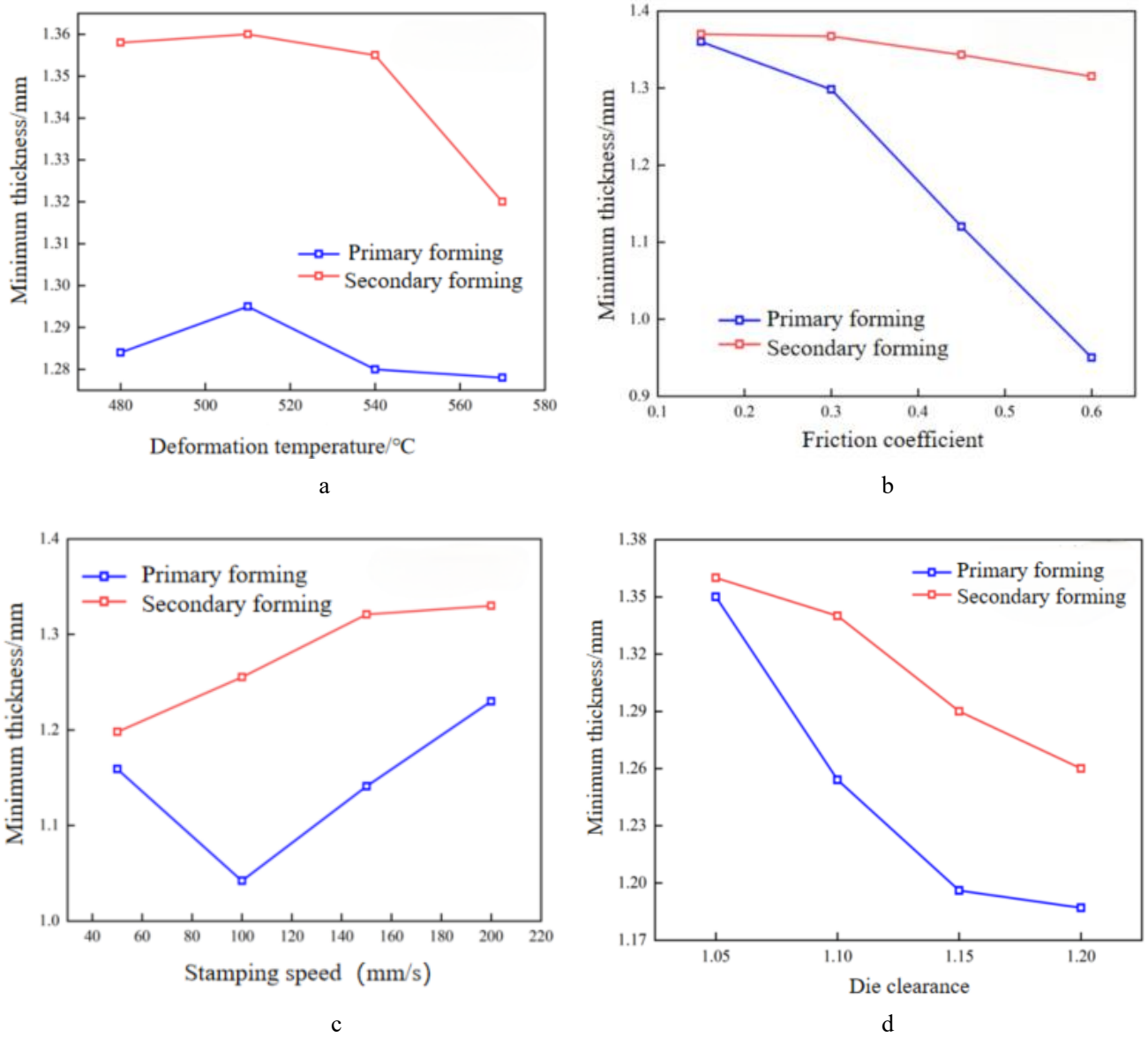


Fig. 11 Influence of process parameters on minimum thickness of rear windshield lower crossbeam: a – deformation temperature, b – friction coefficient, c – stamping speed, d – die clearance

speed, the minimum thickness of the two-step formed parts increased linearly. It is worth mentioning that for the one-step forming process, only when the stamping speed exceeded 100 mm/s, the minimum thickness of the part increased with the increase of the stamping speed. This indicated that when the stamping speed reached a certain degree, the heat dissipation could be reduced, which was conducive to the uniform flow of the material.

Fig. 11, d shows the change curves of the minimum thickness of rear windshield lower crossbeam of aluminum alloy automobiles under different die clearances. Under the same die clearance, the minimum thickness of the two-step formed parts was greater than that of the one-step formed parts. With the increase of die clearance, the minimum thickness of parts decreased and the maximum thinning rate increased. Compared with the two-step forming, the influence of the die clearance on the thinning of the parts is more significant using the one-step forming. When the die clearance was 1.05t, the minimum thickness of the parts under the two forming methods was relatively close, and the maximum thinning rate was between 9% and 10%. With the increase of die clearance, both the curves of the two forming methods declined obviously. When the die clearance was 1.20t, the maximum thinning rate of the one-step formed parts was 21%, and that of the two-step formed parts was 16%.

## 5. Multi-Objective Optimization of Process Parameters

### 5.1. Gradient boosting regression tree machine learning model

The maximum thickening rate and the maximum thinning rate of a part are usually used as important evaluation indexes to judge the wrinkle and crack failure. In order to accurately reflect the highly nonlinear relationship between hot stamping process parameters and the maximum thickening rate and maximum thinning rate of parts, machine learning algorithm was used to establish the prediction model of the maximum thickening rate and maximum thinning rate. Latin hypercube sampling (LHS) was used to build sample data sets. The principle of LHS is to divide each independent variable into several intervals of equal spacing, and randomly select points as sampling points in each interval to finally compose sample sampling results [39]. It can reduce the number of sample points as much as possible while ensuring the uniform distribution of sample points, especially for large sample sampling. The range of process parameters was set as shown in Table 3. 300 samples were collected from the range of parameters using LHS method, and python code was used to control the solver for automatic simulation.

The specific steps are as follows: Fig. 12 shows the recognition sample of the simulation results image. The maximum and minimum thickness values in the simulation results need to be extracted, namely the values 1.695 and 1.149 in the red box. The Opencv module in the open source program Python was used for binary processing to extract image pixels in the fixed area of the image, and then Pytesseract, the OCR character recognition module in Python, was used for digital extraction. The images of the simulation results were stored in the folder in order. Since each picture was of the same size, it was only necessary to


Fig. 12 Recognition sample of the simulation results image

Table 3

Range of LHS process parameters

| Process parameter | Forming temperature $T$, °C | Friction coefficient $\mu$ | Stamping speed $V$, mm/s | Die clearance $\lambda$, mm |
|---|---|---|---|---|
| Sampling upper bound | 480 | 0.05 | 50 | 1.05t |
| Sampling lower bound | 570 | 0.60 | 500 | 1.20t |

digitally identify the position of the red box shown in the sample image to obtain the corresponding results of each group of process parameters.

Using Eq. (1), the identified values were converted to the maximum thickening rate $\eta$ and the maximum thinning rate $\tau$:

$$\left.\begin{aligned}\eta &= \frac{E_{max}-E}{E}\times 100\%,\\ \tau &= \frac{E-E_{min}}{E}\times 100\%,\end{aligned}\right\}, \tag{1}$$

where, $E$ is the thickness of the original sheet, $E_{max}$ is the maximum thickness of the formed part, and $E_{min}$ is the minimum thickness of the formed part. The complete set of identified data is provided in Table 4.

Before machine learning model training, the max-min normalization method was used to normalize the sample data set, and the data was converted into dimensionless form, so that the model prediction results could converge more quickly and the training speed was faster. The data was converted to the range of interval [0,1] using Eq. (2).

$$\bar{x} = \frac{x-x_{min}}{x_{max}-x_{min}}, \tag{2}$$

where, $\bar{x}$ is the normalized data, $x$ is the original data, $x_{min}$ is the minimum value in the original data, and $x_{max}$ is the maximum value in the original data. At the same time, the sample data set was divided into the training set and the test set according to the ratio of 8:2, and the sample order was shuffled.

Gradient boosting regression tree (GBRT) is a machine integrated learning algorithm proposed by Friedman for regression, classification and ranking tasks [40]. GBRT algorithm uses Classification and Regression Tree (CART) as the basic learner, and each CART tree learns to fit the residual of the previous CART tree until a specified number of CART trees are generated or the error is below the set value. GBRT algorithm adjusts the parameters of each tree by gradient descent method similar to neural network to gradually reduce the training error of the current data set.

Table 4

Sample set of process parameter

| No. | Training sample parameter values | | | | | |
|---|---|---|---|---|---|---|
| | Forming temperature $T$, °C | Friction coefficient $\mu$ | Stamping speed $V$, mm/s | Die clearance $\lambda$, mm | Maximum thickening rate $\eta$,% | Maximum thinning rate $\tau$, % |
| 1 | 547.939 | 0.361 | 289.655 | 1.10t | 15.067 | 23.600 |
| 2 | 491.791 | 0.191 | 411.231 | 1.10t | 13.200 | 18.867 |
| 3 | 563.909 | 0.301 | 465.939 | 1.10t | 4.530 | 6.267 |
| 4 | 532.425 | 0.219 | 156.389 | 1.15t | 13.730 | 36.200 |
| 5 | 534.673 | 0.517 | 279.150 | 1.20t | 13.400 | 27.467 |
| 6 | 511.738 | 0.245 | 339.290 | 1.05t | 13.677 | 17.067 |
| 7 | 550.006 | 0.514 | 371.394 | 1.05t | 4.867 | 10.000 |
| 8 | 551.614 | 0.109 | 61.797 | 1.10t | 11.334 | 31.400 |
| 9 | 515.508 | 0.072 | 122.708 | 1.15t | 21.267 | 32.134 |
| 10 | 496.446 | 0.543 | 362.932 | 1.10t | 13.467 | 28.134 |
| 11 | 488.285 | 0.053 | 392.877 | 1.05t | 8.800 | 12.134 |
| 12 | 537.012 | 0.284 | 80.356 | 1.20t | 7.600 | 47.867 |
| 13 | 504.923 | 0.084 | 384.234 | 1.20t | 11.600 | 22.667 |
| … | … | … | … | … | … | … |
| 300 | 492.886 | 0.379 | 93.771 | 1.10t | 15.334 | 38.400 |

For the Optimization problem of loss function $H(\theta)$ with a single variable, the variable $\theta$ is added in the direction of minimum gradient in each update iteration, and $H(\theta)$ gradually reaches local optimization in each iteration of parameter update. When $H(\theta)$ is locally optimal, the optimal $\theta$ is then determined, as shown in Eq. (3):

$$\theta_t = \theta_{t-1} - \partial \frac{\partial}{\partial \theta} H(\theta). \tag{3}$$

In Eq. (3), $\alpha$ is the learning rate, $\theta$ is the parameter.

The variable $\theta$ is extended to the entire feature space, that is, for the entire GBRT algorithm, the estimate of the first m CART trees is obtained, and the Eq. (4) can be obtained by using gradient descent method:

$$f_m(x) = f_{m-1}(x) - \alpha h_m(x). \tag{4}$$

In Eq. (4), $f_m(x)$ is the estimated value of the first m CART trees, $f_{m-1}(x)$ is the estimate of the previous $m$-1 CART tree, $\alpha$ is the learning rate and $h_m(x)$ is the loss function.

The loss function of GBRT was set as root mean square error (RMSE), and the specific hyper-parameter were set as shown in Table 5.

Table 5

GBRT hyper-parameter settings

| Hyper-parameter | Learning rate | Basic model | Number of trees | Depth of tree |
|---|---|---|---|---|
| Set value | 0.1 | Decision tree | 99 | 4 |

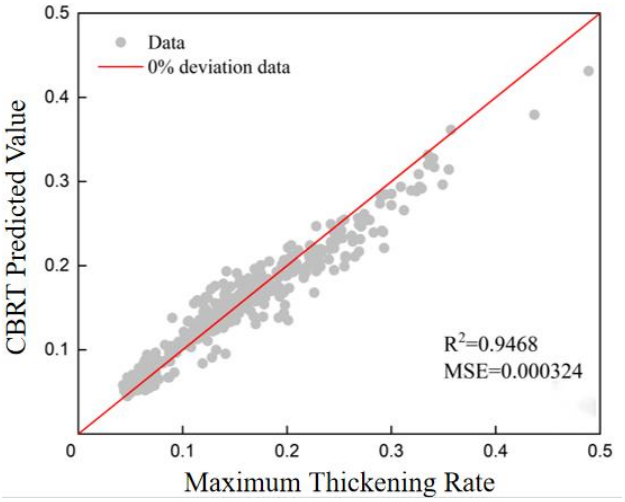


a

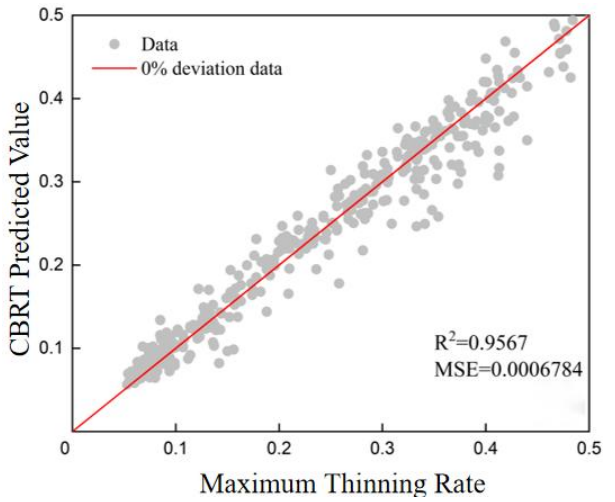


b

Fig. 13 Comparison between GBRT model and experiment: a – maximum thickening rate, b – maximum thinning rate

Taking coefficient of determination ($R^2$) and mean square error (MSE) as evaluation indexes, the results of maximum thinning rate and maximum thickening rate are shown in Fig. 13. The $R^2$ of the GBRT model is close to 1, which means that the model can explain the variation in the data very well. At the same time, the validity of GBRT model applied to the modeling of maximum thinning rate and maximum thickening rate was verified in the acceptable range of MSE.

### 5.2. Multi-objective optimization based on NSGA-II algorithm

The Non-dominated Sorting Genetic Algorithm II (NSGA-II) is a multi-objective optimization algorithm based on biogenetics. In order to obtain the multi-objective optimization solution of the hot stamping formability of the rear windshield lower crossbeam of 6016 aluminum alloy automobile, the established GBRT model was as the objective function $F(x)$ to optimize, which contained two sub-functions, namely the maximum thinning rate and the maximum thickening rate. Usually, when the maximum thickening rate of aluminum alloy hot stamping parts is less than 10%, the maximum thinning rate is less than 20%, the parts show good formability. Optimization parameters include stamping speed $x_1$, die clearance $x_2$, sheet initial forming temperature $x_3$ and friction coefficient $x_4$. The constraints of optimization parameters are shown in Eq. (5).

In Eq. (5), *GBRT* is the proxy model of GBRT of the thickening rate and thinning rate of 6016 aluminum alloy, $M$ and $N$ are the output matrices, $M*GBRT(X)$ is the maximum thickening rate output of the GBRT model, $N*GBRT(X)$ is the maximum thinning rate output of the GBRT model.

$$\left.\begin{aligned} &min\,F(X)=\left[M*GBRT(X);\,N*GBRT(X)\right];\\ &\left(M=[1,0];\,N=[0,1]\right);\\ &X=\left[x_1,x_2,x_3,x_4\right]^T;\\ &50\le x_1\le 500;\\ &x_2\in\left[1.05t,1.10t,1.15t,1.20t\right];\ \left(t=1.5mm\right);\\ &480\le x_3\le 570;\\ &0.05\le x_4\le 0.60. \end{aligned}\right\} \quad (5)$$

After iterative operation, the optimal data set obtained is shown in Fig. 14. It can be found that the maximum thickening rate of all Pareto solution sets is less than 7%, and the maximum thinning rate of that is less than 10%. Because of the fractional number processing, there is a weak domination relationship in the solution set, but in fact a non-domination relationship. The optimal solution of the hot stamping forming process parameters of the rear windshield lower crossbeam of the 6016 aluminum alloy automobile is

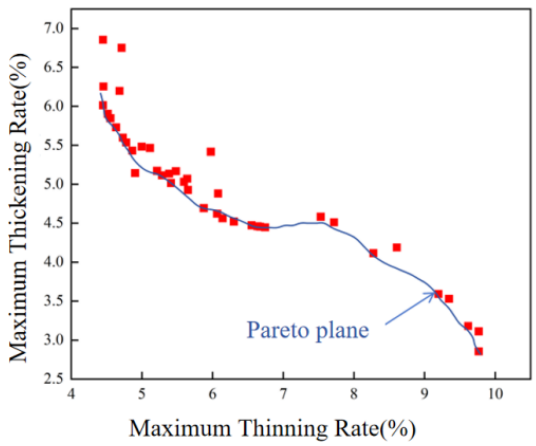


Fig. 14 Optimal solution set for maximum thickening rate and maximum thinning rate of parts

Table 6
Optimum process parameters for hot stamping of rear windshield lower crossbeam

| Process parameter | Forming temperature, °C | Friction coefficient | Stamping speed, mm/s | Die clearance, mm |
|---|---|---|---|---|
| Optimal value | 568.867 | 0.1502 | 450.717 | 1.05t |

shown in Table 6. In order to obtain the best match between the maximum thickening rate and the maximum thinning rate of the formed part, the optimal forming process parameters should be selected as follows: a forming temperature of 570°C, a friction coefficient of 0.15, a stamping speed of 450 mm/s, and a die clearance of 1.05t.

## 6. Conclusions

In this paper, the integrated application of new process, simulation prediction, die development, and intelligent optimization has been implemented in a typical automotive component forming study. An innovative composite hot stamping forming process combining cold die forming with synchronous quenching was applied to the rear windshield lower crossbeam, a typical automotive body component. This study explored the feasibility of using this new process for forming complex automotive parts and proposed a two-step forming method based on the part's geometric characteristics and forming challenges. Finite element simulations were conducted to compare the formability of the part under two forming methods and analyzed how process parameters affected thickness distribution. By developing a set of segmented hot stamping die with cooling system, two forming methods can be achieved using a set of die. Building on this foundation, a gradient-boosted regression tree machine learning model and NSGA-II algorithm were employed to optimize hot stamping process parameters through multi-objective optimization. This approach offers an efficient, precise, and cost-effective solution for digitalizing and intelligentizing the forming process of aluminum alloy automotive components. The conclusions drawn from this study are as follows:

The finite element simulation model of hot stamping of the rear windshield lower crossbeam of aluminum alloy automobiles was established. The results showed that the parts using the one-step direct forming had a greater risk of wrinkling and cracking, especially the middle convex position of the part was the most serious thinning. By using the two-step forming process, the thickness distribution of the parts showed a better consistency. Compared with the one-step forming method, the maximum thickening rate and the maximum thinning rate of the two-step formed parts were reduced by 6.1% and 24.8% respectively. The average temperature of the two-step formed parts at the end of the forming was about 100°C lower than that of the one-step formed parts, which significantly improved the efficiency of quenching while using the die forming.

A modular hot stamping die was designed for the rear windshield lower crossbeam, which can realize both the one-step forming and the two-step forming. The experimental results showed that cracks appeared in the middle convex position of parts using one-step forming, while all

qualified parts were obtained using two-step forming at temperatures between 480-570°C The simulation results for the thickness distribution of the part were in good agreement with the experimental data, confirming the precision of the simulation model.

The effects of hot stamping process parameters on the rear windshield lower crossbeam of aluminum alloy automobiles under two different forming methods was compared. The results showed that the choice of forming method can significantly affect the thickness of parts under the same process conditions. Notably, the minimum thickness of the two-step formed parts exceeded that of the one-step formed parts. A gradient boosting regression tree machine learning model was developed to predict the maximum thickening rate and maximum reduction rate of the parts. By employing the NSGA-II multi-objective optimization algorithm, an optimal set of process parameters for hot stamping of the rear windshield lower crossbeam was determined, suggesting a forming temperature of 570°C, a friction coefficient of 0.15, a stamping speed of 450 mm/s, and a die clearance of 1.05t.

## Funding

This study was supported by the "Pioneer" R&D Program of Zhejiang (Grant No. 2023C01090) and the Graduate Research and Innovation Fund of Zhejiang University of Science and Technology (Grant No. 0101320464).

## References

1. **Wang, Y.; Hao, Y.; Hou, Y. L.; Quan, Q.; Li, Y. Z.** 2024. Optimizing scope 3 emissions in the automotive manufacturing industry: a multidisciplinary approach, Carbon Research 3(1): 49. https://doi.org/10.1007/S44246-024-00131-2.
2. **Candela, A.; Sandrini, G.; Gadola, M.; Chindamo, D.; Magri, P.** 2024. Lightweighting in the automotive industry as a measure for energy efficiency: Review of the main materials and methods, Heliyon 10(8): e29728. https://doi.org/10.1016/j.heliyon.2024.e29728.
3. **Miller, W. S.; Zhuang, L.; Bottema, J.; Wittebrood, A. J.; Smet, P. D.; Haszler, A.; Vieregge, A.** 2000. Recent development in aluminum alloys for the automotive industry, Materials Science and Engineering: A 280(1): 37-49. https://doi.org/10.1016/S0921-5093(99)00653-X.
4. **Xiong, F.; Zou, X. H.; Zhang, Z. G.; Shi, X. H.** 2020. A systematic approach for multi-objective lightweight and stiffness optimization of a car body, Structural and Multidisciplinary Optimization 62(6): 3229-3248. https://doi.org/10.1007/s00158-020-02674-5.
5. **Cecchel, S.** 2020. Materials and Technologies for Lightweighting of Structural Parts for Automotive Applications: A Review, SAE International Journal of Materials and Manufacturing 14(1): 81-97. https://doi.org/10.4271/05-14-01-0007.
6. **Zhang, W.; Xu, J.** 2022. Advanced lightweight materials for Automobiles: A review, Materials and Design 221: 110994. https://doi.org/10.1016/j.matdes.2022.110994.
7. **Zhan, H. Y.; Zeng, G.; Wang, Q. G.; Wang, C. J.; Wang, P.; Wang, Z.; Xu, Y. W.; Hess, D.; Crepeau, P.; Wang, J. F.** 2023. Unified casting (UniCast) aluminum alloy—a sustainable and low-carbon materials solution for vehicle lightweighting, Journal of Materials Science and Technology 154: 251-268. https://doi.org/10.1016/j.jmst.2023.02.003.
8. **Chang, J. K.; Takata, K.; Ichitani, K.; Taleff, E. M.** 2010. Ductility of an aluminum-4.4wt.pct.magnesium alloy at warm and hot working temperatures, Materials Science and Engineering: A 527(16-17): 3822-3828. https://doi.org/10.1016/j.msea.2010.02.042.
9. **Cui, M. M.; Wang, Z.; Wang, L. G.; Huang, Y.** 2020. Numerical Simulation and Multi-Objective Optimization of Partition Cooling in Hot Stamping of the Automotive B-Pillar Based on RSM and NSGA-II, Metals 10(9): 1264. https://doi.org/10.3390/met10091264.
10. **Zhang, Z. Q.; Ouyang, X.; Zhu, L. J.** 2022. Study on the hot stamping simulation and experiment of A-pillar patchwork blanks, The International Journal of Advanced Manufacturing Technology 122(1): 365-376. https://doi.org/10.1007/s00170-022-09694-z.
11. **Wang, A. L.; Liu, J.; Gao, H. X.; Wang, L. L. Masen M.** 2017. Hot stamping of AA6082 tailor welded blanks: Experiments and knowledge-based cloud – finite element (KBC-FE) simulation, Journal of Materials Processing Technology 250: 228-238. https://doi.org/10.1016/j.jmatprotec.2017.07.025.
12. **Harrion, N. R.; Luckey, S. G.** 2014. Hot Stamping of a B-Pillar Outer from High Strength Aluminum Sheet AA7075, SAE International Journal of Materials and Manufacturing 7(3): 567-573. https://doi.org/10.4271/2014-01-0981.
13. **Zhou, J.; Wang, B. Y.; Lin, J. G.; Fu, L.** 2013. Optimization of an aluminum alloy anti-collision side beam hot stamping process using a multi-objective genetic algorithm, Archives of Civil and Mechanical Engineering 13(3): 401-411. https://doi.org/10.1016/j.acme.2013.01.008.
14. **Jiang, B. H.; Huang, J. H.; Ma, H. P.; Zhao, H. J.; Ji, H. C.** 2022. Multi-Objective Optimization of Process Parameters in 6016 Aluminum Alloy Hot Stamping Using Taguchi-Grey Relational Analysis, Materials 15(23): 8350. https://doi.org/10.3390/ma15238350.
15. **Shang, H. C.; Wu, P. F.; Lou, Y. S.; Wang, J. Z.; Chen, Q.** 2022. Machine learning-based modeling of the coupling effect of strain rate and temperature on strain hardening for 5182-O aluminum alloy, Journal of Materials Processing Technology 302: 117501. https://doi.org/10.1016/j.jmatprotec.2022.117501.
16. **Ying, L.; Gao, T. H.; Rong, H.; Han, X.; Hu, P.; Hou, W. B.** 2019. On the thermal forming limit diagram (TFLD) with GTN mesoscopic damage model for AA7075 aluminum alloy: Numerical and experimental investigation, Journal of Alloys and Compounds 802: 675-693. https://doi.org/10.1016/j.jallcom.2019.05.342.
17. **Ivanoff, T. A.; Carter, J. T.; Hector, L. G.; Taleff, E. M.** 2019. Retrogression and Reaging Applied to Warm Forming of High-Strength Aluminum Alloy AA7075-T6 Sheet, Metallurgical and Materials Transactions A-Physical Metallurgy and Materials Science 50(3): 1545-1561. https://doi.org/10.1007/s11661-018-5084-3.
18. **Fan, X. B.; He, Z. B.; Yuan, S. J.; Lin, P.** 2013. Investigation on strengthening of 6A02 aluminum alloy sheet in hot forming-quenching integrated process with warm

forming-dies, Materials Science and Engineering: A 587: 221-227.
https://doi.org/10.1016/j.msea.2013.08.059.

19. **Wang, L.; Strangwood, M.; Balint, D.; Lin, J.; Dean, A. T.** 2011. Formability and failure mechanisms of AA2024 under hot forming conditions, Materials Science and Engineering: A 528(6): 2648-2656.
https://doi.org/10.1016/j.msea.2010.11.084.
20. **Gu, R. Y.; Liu, Q.; Chen, S. C.; Wang, W. R.; Wei, X. C.** 2019. Study on High-Temperature Mechanical Properties and Forming Limit Diagram of 7075 Aluminum Alloy Sheet in Hot Stamping, Journal of Materials Engineering and Performance 28(2): 7259-7272.
https://doi.org/10.1007/s11665-019-04436-x.
21. **Jiang, F. Q.; Huang, J. W.; Tang, L.; Wang, F. X.; Xiao, Q. F.; Yin, Z. M.** 2019. Effects of Quench Rate on Mechanical Properties and Microstructures of High-Strength 7046A Aluminum Alloy, JOM 71(5): 1722-1730.
https://doi.org/10.1007/s11837-018-3153-0.
22. **Jiang, Y. F.; Ding, H.** 2020. Investigations into Hot Form Quench Conditions on Microstructure Evolution and Bake-Hardening Response for High-Strength Aluminum Alloy, Journal of Materials Engineering and Performance 29(12): 8331-8339.
https://doi.org/10.1007/s11665-020-05245-3.
23. **El Fakir, O.; Wang, L. L.; Balint, D.; Dear, P. J.; Lin, J. G.; Dean, T. A.** 2014. Numerical study of the solution heat treatment, forming, and in-die quenching (HFQ) process on AA5754, International Journal of Machine Tools and Manufacture 87: 39-48.
https://doi.org/10.1016/j.ijmachtools.2014.07.008.
24. **Zhou, J.; Yang, X. M.; Mu, Y. H.; Liu, S. Q.; Wang, B. Y.** 2021. Numerical simulation and experimental investigation of tailored hot stamping of boron steel by partial heating, Journal of Materials Research and Technology 14: 1347-1365.
https://doi.org/10.1016/j.jmrt.2021.07.025.
25. **Sirvin, Q.; Velay, V.; Bonnaire, R.; Penazzi, L.** 2019. Mechanical behaviour modelling and finite element simulation of simple part of Ti-6Al-4V sheet under hot/warm stamping conditions, Journal of Manufacturing Processes 38: 472-482.
https://doi.org/10.1016/j.jmapro.2018.12.010.
26. **Bilir, O. G.; Aycan Başer, T.; Karşı, A.; Bayram, A.; Erişir, E.** 2022. Modeling and simulation of hot stamping process for medium manganese steel alloy, International Journal of Material Forming 15(5): 67.
https://doi.org/10.1007/s12289-022-01707-2.
27. **Liu, K.; Zhang, B. M.; Xu, X. Y.; Ye, J. R.; Liu, C. X.** 2019. Simulation and Analysis of Process-Induced Distortions in Hemispherical Thermostamping for Unidirectional Thermoplastic Composites, Polymer Composites 40(5): 1786-1800.
https://doi.org/10.1002/pc.24936.
28. **Xiao, W. C.; Wang, B. Y.; Kang, Y.; Ma, W. P.; Tang, X. F.** 2017. Deep drawing of aluminum alloy 7075 using hot stamping, Rare Metals 36(6): 485-493.
https://doi.org/10.1007/s12598-017-0919-4.
29. **Ma, W. Y.; Wang, B. Y.; Fu, L.; Zhou, J.; Huang, M. D.** 2015. Effect of friction coefficient in deep drawing of AA6111 sheet at elevated temperatures, Transactions of Nonferrous Metals Society of China 25(7): 2342-2351.
https://doi.org/10.1016/S1003-6326(15)63849-3.
30. **Ghiotti, A.; Simonetto, E.; Bruschi, S.** 2019. Influence of process parameters on tribological behaviour of AA7075 in hot stamping, Wear 426-427(Pt A): 348-356.
https://doi.org/10.1016/j.wear.2018.11.031.
31. **Li, J. B.; Chen, X. H.; Liu, X. L.** 2021. Investigation of process parameters and plate local thickening on residual stresses in hot stamping process, Mechanics and Industry 22: 18.
https://doi.org/10.1051/meca/2021015.
32. **Deb, K.; Pratap, A.; Agarwal, S.; Meyarivan, T.** 2002. A fast and elitist multiobjective genetic algorithm: NSGA-II, IEEE Transactions on Evolutionary Computation 6(2): 182-197.
https://doi.org/10.1109/4235.996017.
33. **Decke, J.; Engelhardt, A.; Rauch, L.; Degener, S.; Sajadifar, S.V.; Scharifi, E.; Steinhoff, K.; Niendorf, T.; Sick, B.** 2022. Predicting Flow Stress Behavior of an AA7075 Alloy Using Machine Learning Method, Crystals 12(9): 1281.
https://doi.org/10.3390/cryst12091281.
34. **Xie, Y. M.; Du, L. F.; Zhao, J. B.; Liu, C.; Li, W.** 2021. Multi-objective optimization of process parameters in stamping based on an improved RBM–BPNN network and MOPSO algorithm, Structural and Multidisciplinary Optimization 64(6): 4209-4235.
https://doi.org/10.1007/s00158-021-03056-1.
35. **Liu, X. C.; Cai, Z. H.; Zheng, Y.; El Fakir, O.; Gandra, J.; Wang, L. L.** 2020. A general IHTC model for hot/warm aluminum stamping, Applied Thermal Engineering 181: 115619.
https://doi.org/10.1016/j.applthermaleng.2020.115619.
36. **Zhang X. K.** 2020. Experimental and Finite Element Simulation Study of Hot Stamping of 7075 Aluminum Alloy Using Warm Die, Jilin University (Chinese Academic Thesis).
https://doi.org/10.27162/d.cnki.gjlin.2020.006875.
37. **Huang X. M.** 2024. Research on formability and quenching strengthening of 2195 Al-Li alloy during hot stamping, Beijing University of Science and Technology (Chinese Academic Thesis).
https://doi.or g/10.26945/d.cnki.gbjku.2024.000025.
38. **Shinde, P. P.; Shah, S.** 2018. A Review of Machine Learning and Deep Learning Applications C// 2018 Fourth international conference on computing communication control and automation (ICCUBEA) IEEE: 1-6.
https://doi.org/10.1109/ICCUBEA.2018.8697857.
39. **Zhang, Y. R.; Haghani, A.** 2015. A gradient boosting method to improve travel time prediction, Transportation Research Part C: Emerging Technologies 58: 308-324.
https://doi.org/10.1016/j.trc.2015.02.019.

H. Zhao, J. Xu, J. Huang, Y. Xiao, H. Fu, B. Jiang

SIMULATION AND OPTIMIZATION FOR HOT STAMPING PROCESS OF REAR WINDSHIELD LOWER CROSSBEAM OF ALUMINUM ALLOY AUTOMOBILES

S u m m a r y

The simulation of the hot stamping process for the rear windshield lower crossbeam in aluminum alloy automobiles was carried out. Contrasted with the one-step forming process, the maximum thickness increase rate was lowered by 6.1% and the maximum thinning rate was decreased by 24.8% using the two-step forming process. Under identical process parameters, the minimum thickness of two-step formed parts was greater than that of one-step formed parts. The forming experiment was conducted by employing the self-developed modular hot stamping die. A gradient boosting regression tree machine learning model for the maximum thickening rate and the maximum reduction rate of the parts was established, and the optimal process parameters matching for the hot stamping of the rear windshield lower crossbeam were obtained based on the NSGA-II multi-objective optimization algorithm, namely, forming temperature 570°C, friction coefficient 0.15, stamping speed 450 mm/s and die clearance 1.05t.

**Keywords:** aluminum alloy, hot stamping, machine learning, process optimization, mechanical simulation.

Received January 10, 2025
Accepted February 20, 2026